Fracture Process Zone Analysis of Concrete Using Moiré Interferometry

by S. He, Z. Feng and R. E. Rowlands

ABSTRACT— The fracture process zone (FPZ) ahead of a crack tip in concrete and mortar beams subjected to three-point bending was studied using moiré interferometry. A large FPZ can occur in concrete before the external load reaches its maximum value. Comparing the experimental results between concrete and mortar suggests that the aggregate contributes to the formation of the large FPZ in concrete. The formation of this large FPZ makes concrete less brittle than mortar. The effect of the FPZ on the fracture property, such as stress intensity factor, is investigated by combining moiré interferometry measured displacements with the smoothing FEM method. The study shows that a large FPZ significantly affects the value of the stress intensity factor.

Introduction

The development of large fracture process zones (FPZs) is an important characteristic of the fracture of concrete. The FPZ renders classical LEFM (linear elastic fracture mechanics) unsuitable for analyzing concrete structures and complicates the assessment of fracture toughness of concrete. Considering this FPZ, researchers have tended to adopt one of the following three different approaches for analyzing concrete fracture: (1) use the concepts of stress intensity factor and energy release rate when the FPZ is small (this condition can be satisfied for some concrete structures), (2) employ special nonlinear fracture models that are based on concepts of LEFM, (3) use nonlinear fracture mechanics approaches directly. The first approach necessitates knowing the size of the FPZ to justify using classical LEFM concepts. The second concept involves introducing the idea of an effective crack. The size of this effective crack is directly related to the size of the FPZ. Nonlinear fracture models usually mathematically account for the softening damage of the fracture process zone in the form of either a stress displacement relationship or a stress-strain relation. All of the above techniques require knowing the characteristics of the FPZ. Moiré interferometry is employed here to study and to better understand this fracture process zone in concrete.

In view of the comments above, fracture process zone analysis has become a very important aspect of fracture mechanics of concrete. Objectives of previous research appear to have emphasized determining the size of the FPZ, studying the stress distribution inside the FPZ and investigating the influence of the FPZ on the stress intensity factor or energy release rate. Methods used in these analyses include FEM modeling and direct and indirect testing.

Well-known fracture models involving nonlinear FEM studies of the FPZ include the fictitious crack model by Hillerborg[1] and the crack band model by Bazant.[2] These models represent the fracture process zone or microcrack zone by a damage band or a band of crack-closing forces. The closing forces can be determined from the postpeak stress displacement relationship of the uniaxial tensile test. Recognizing the difficulties in conducting the direct tension test, the postpeak stress displacement relationships are sometimes assumed to be linear or bilinear. The search for a good stress displacement relationship inside the FPZ becomes the focus of such an investigation. The finite element method (FEM) is often used to compare the results of different models.[3–9] Some approaches combine direct experimental analyses with the FEM method[10–13] or with the J-integral.[14] Results of these approaches are promising. However, a better understanding of the FPZ is essential, and additional experimental effort is necessary.

Instead of using a nonlinear model and the stress displacement relationship inside the FPZ, a different approach uses LEFM concepts with an effective crack length. The compliance measurement method of Refs. 15 and 16 is representative of this technique. A different effective crack concept was proposed by Jenq and Shah.[17] They determine the effective crack length so that the crack mouth opening displacement calculated using LEFM at the peak load is equal to the measured elastic crack mouth opening displacement.

Observation of the actual FPZ provides direct information regarding the behavior of the zone. Many relevant investigations have been conducted using various experimental techniques. These include holographic interferometry,[18,19] laser speckle,[20,21] photoelastic coating[22] and moiré interferometry.[10–13,23] Moiré interferometry can be particularly effective because it provides full-field displacement data at high sensitivity and the opportunity for real-time observation of the FPZ progress.

Moiré interferometric analyses of both cracked concrete and mortar beams under three-point bending are considered here. The initial crack length, a, is either 2.54 cm or 5.08 cm (1 in. or 2 in.). Beam dimensions are shown in Fig. 1. The concrete and mortar beams were provided with a 1200 line-per-millimeter moiré phase ruling that is parallel to the crack. The active moiré ruling on the concrete (mortar) was interrogated by a virtual ruling of 2400 lines per millimeter.[24] This gives a moiré interferometric resolution of 416 nm (16.4 $\times 10^{-6}$ in.) per fringe. The moiré fringe patterns reveal de-

S. He, is Research Associate, Applied Superconductivity Center, and Z. Feng, Professor, Jilin University of Technology, Jilin, China. R. E. Rowlands, is Professor of Engineering Mechanics, University of Wisconsin–Madison, Madison WI, 53706,

Original manuscript submitted: April 13, 1994.
Final manuscript received: August 4, 1995.

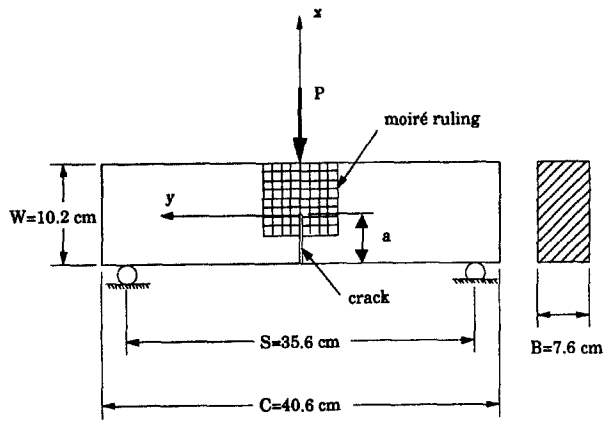

Fig. 1—Three-point bending specimen with crack length a = 2.54 cm or 5.08 cm

tails on the formation and propagation of the microcrack inside the FPZ. This entire process was recorded using both a Hi8 camcorder and photographic film. The smoothing FEM concept[25] was used to process the moiré fringe data.

Experimental Analysis

A series of concrete and mortar beams was tested under three-point bending, and the horizontal displacement data in the neighborhood of the crack tip were recorded using moiré interferometry. The purpose of the tests was to study the fracture process zone in front of the crack tip in the concrete and mortar. Moiré fringe patterns are recorded on photographic film and with an Hi8 camcorder. The loading and the load-point displacements were recorded by a computer through an A/D board. Moiré fringe patterns were also monitored in real time by a TV monitor throughout an entire test. The following section briefly describes some of the experimental details.

Moiré Interferometry

Coherent illumination from an argon ion laser (LEXEL Ion laser model 95) was used. The wavelength of the laser light is $\lambda = 514.5$ nm. The specimen grating is a crossed-line diffraction ruling with a frequency of $F = 1200$ lines/mm. The vertical virtual grating has a frequency of $f = 2400$ lines/mm. Interferometric moiré combines the ± 1 order diffracted beams to generate moiré fringes, and the effective moiré line density is that of the virtual analyzer, i.e., 2400 lines/mm. The displacement of a loaded component is given by

$$v = \frac{1}{f} N, \tag{1}$$

where v is the displacement in the y-direction transverse to the crack, N is the moiré fringe order and f is the frequency of the virtual reference grating. For $f = 2400$ lines/mm, one obtains a relative displacement resolution of 416 nm (16 μ in.) per fringe.

Specimens

The geometry of the three-point bending specimens is shown in Fig. 1. A crack of either 2.54 cm or 5.08 cm (1 in. and 2 in.) in length was molded in the specimens. Both

TABLE 1—THE CONTENT PROPORTIONS OF THE CONCRETE AND MORTAR MIXTURES (BY WEIGHT)

	Concrete	Mortar
Cement	1.0	1.0
Sand	2.6	3.0
Aggregate	3.8	0.0
Water	0.64	0.56

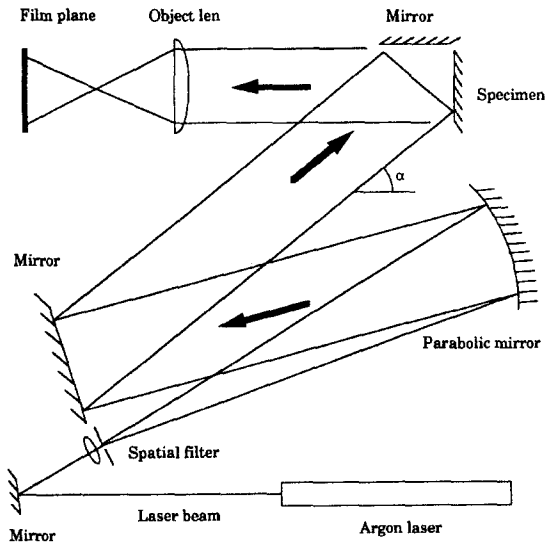

Fig. 2—Setup for moiré interferometry

concrete beams and mortar beams were prepared and tested. The content proportions of the concrete and mortar mixtures are presented in Table 1. Type I Portland cement and Torpedo sand were used. The aggregate is #1 washed stone with aggregate sizes ranging from 0.95 cm to 1.91 cm (0.375 in. to 0.75 in.).

The prepared concrete and mortar specimens were cured in a moist room for 28 days prior to testing. The midspan region of each beam specimen was polished to facilitate application of the diffraction grating (see Ref. 26 for details).

Concrete and mortar cylinders 15 cm × 30 cm (6 in × 12 in.) were made from the same batch of mixtures (and subjected to the same curing conditions) as were the beam specimens. The material properties of these cylinders were measured using conventional techniques, and their values are listed in Table 2.

Experimental Setup

All experiments were carried out on a vibration-isolated optical table. Figure 2 is a schematic sketch of the optical setup; the actual equipment is shown in Fig. 3. A test specimen was supported at two positions along its bottom edge and loaded at the center of the top edge (Fig. 1).

Because displacements perpendicular to the vertical crack surface are of prime interest here, only horizontal displacements that are perpendicular to the crack surface were measured. Figure 4 is a photograph of a typical concrete specimen, including its highly reflective diffraction grating.

Data Acquisition and Processing

During testing, the applied load P and associated load-point displacement δ were measured by a load cell and an

TABLE 2—MEASURED MATERIAL PROPERTIES OF THE CONCRETE AND MORTAR MIXTURES

	E GPa (psi)	ν	f_t kPa (psi)	f_c MPa (ksi)
Mortar	29.4 (4.26e6)	0.2	2.04 (296.2)	61.3 (8.88)
Concrete	34.1 (4.95e6)	0.19	2.08 (302.5)	54.0 (7.84)

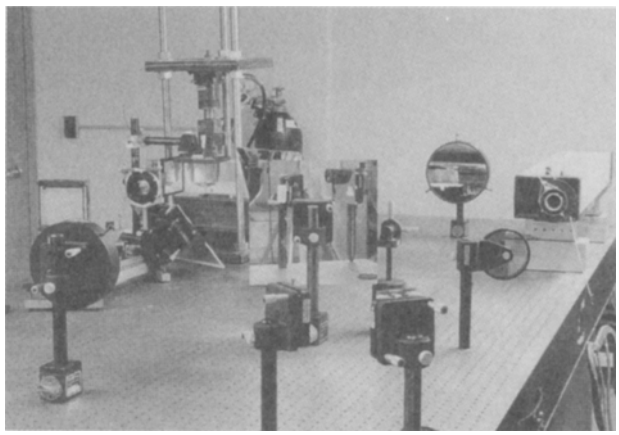

Fig. 3—Optional setup for moiré interferometry

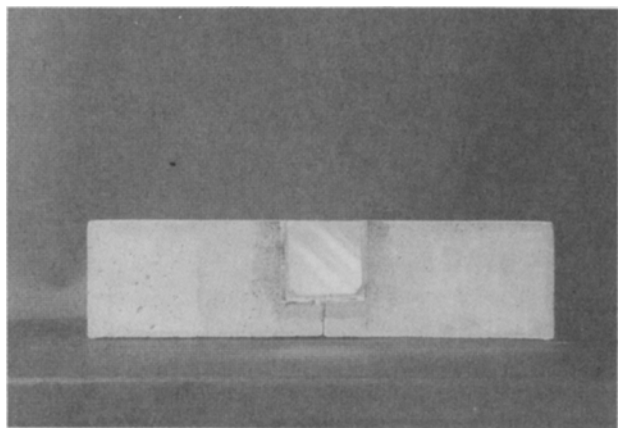

Fig. 4—A concrete specimen and its moiré ruling

LVDT, respectively. The load-point displacement data were recorded by an IBM PC containing a data acquisition board (DT2801 A/D). A special data acquisition software program was developed as part of this research to control the A/D board. The program is able to display the P-δ curve in real time during an actual test.

The moiré fringes were recorded on Polaroid positive-negative 4 × 5 instant sheet films using a film holder model 545. To help monitor the fringe patterns and to assist synchronizing the photography, a Sony TV monitor was also used in conjunction with an Hi8 camcorder. The camcorder recorded the fringe patterns throughout the entire loading process. The magnitude of the applied load corresponding to the moiré fringe patterns was also recorded with the camcorder.

Experimental Results

Representative moiré fringe photographs are shown in Figs. 5 and 6, and test results are in Table 3. Table 3 contains the load P_{FPZ} at which microcracks were first evident in the moiré patterns, the maximum load P_{max}, the length

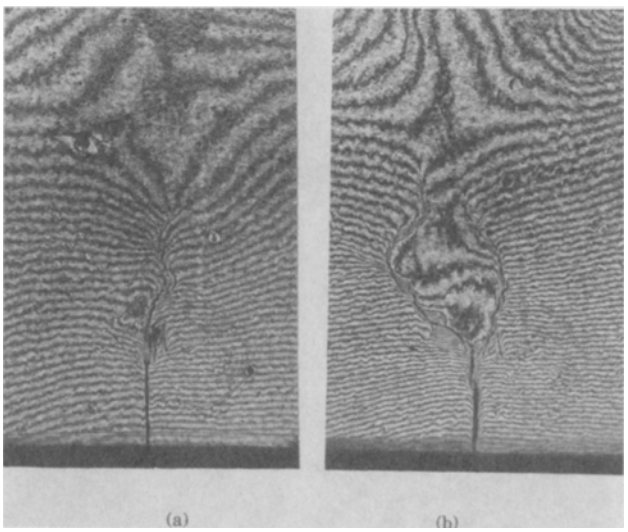

Fig. 5—Representative moiré fringe patterns of concrete with initial crack length of 5.08 cm (2 in.): (a) Specimen #1 at load P = 2.40 kN(540 lb), (b) specimen #2 at load P = 2.42 kN (543 lb)

(size) L_{FPZ} of the FPZ immediately before specimen failure and the ratio P_{FPZ}/P_{max}. The length of the FPZ is observed as the length of a moiré fringe discontinuity region ahead of the crack tip. One can make the following observations from Table 3. (1) A large fracture process zone (FPZ) develops before the external load reaches its maximum value. (2) The length of the FPZ is not a material property. Its value depends on the geometry (i.e., relative length of initial crack) of the specimen (at least in the case of mortar beams). The load at which the FPZ initiates is also geometry (i.e., relative length of initial crack) dependent. (3) Concrete beams have a substantially longer FPZ than do the mortar beams. This suggests that aggregates in concrete increase the FPZ size, which contributes to make concrete much less brittle than mortar.

Figures 5 and 6 show representative moiré fringe patterns for the concrete and mortar beams with a 5.08-cm (2-in.) crack. All of the fringe patterns demonstrate the large fracture process zone ahead of the crack tip before the external load reaches its maximum value P_{max}.

Stress Intensity Factor Computation Using Smoothing FEM

Moiré data reveal that the concrete/mortar specimens have a very large fracture process zone (FPZ) ahead of the crack tip before the applied load reaches its maximum value. Knowledge of the influence of the FPZ on the stress intensity factor is necessary if one is to consider applying LEFM concepts to concrete.

Under LEFM assumptions, the stress intensity factor K_I for a three-point bending beam (Fig. 1) can be computed

TABLE 3—TEST RESULTS ON THE FPZ BY MOIRÉ INTERFEROMETRY MIXTURES

	P_{FPZ} kN (lb)	P_{max} kN (lb)	L_{FPZ} cm (in.)	P_{FPZ}/P_{max}
Mortar beam with 2.54-cm crack	3.53 (795)	4.2 (938)	2.37 (0.93)	85 percent
Mortar beam with 5.08-cm crack	1.31 (296)	2.47 (556)	1.91 (0.75)	53 percent
Concrete beam with 2.54-cm crack	3.55 (798)	4.84 (1088)	3.56 (1.4)	73 percent
Concrete beam with 5.08-cm crack	1.67 (376)	2.50 (562)	3.56 (1.4)	67 percent

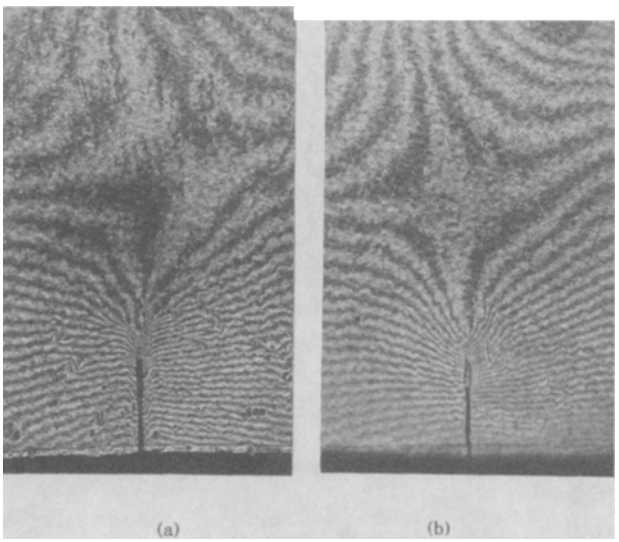

Fig. 6—Representative moiré fringe patterns of mortar with crack length of 5.08 cm (2 in): (a) specimen #7 at load P = 2.54 kN (572 lb), (b) specimen #8 at load P = 2.39 kN (538 lb)

from[27]

$$K_I = \frac{PS}{BW^{\frac{3}{2}}}\left[2.9\left(\frac{a}{W}\right)^{\frac{1}{2}} - 4.6\left(\frac{a}{W}\right)^{\frac{3}{2}} + 21.8\left(\frac{a}{W}\right)^{\frac{5}{2}} - 37.6\left(\frac{a}{W}\right)^{\frac{7}{2}} + 38.7\left(\frac{a}{W}\right)^{\frac{9}{2}}\right] \quad (2)$$

The extent of the FPZ in the concrete/mortar specimens could invalidate application of this formula to the three-point bending tests conducted here. The crack tip quarter-point elements and following displacement equation[28,29] can also be used to compute stress intensity factor K_I when the size of the FPZ is small. Equation (3) can be used to evaluate the effect of FPZ on stress intensity factor when large FPZ is involved, which will be shown later.

$$K_I = \frac{E}{(\kappa+1)(1+\nu)}\sqrt{\frac{\pi}{2L}}\{4v_{b2} - v_{c2} - 4v_{b1} + v_{c1}\}, \quad (3)$$

where the respective v of eq (3) are the opening displacements at the crack tip surface with respect to the local crack tip coordinate system (Figs. 1 and 7). L is the length of the crack tip element along the crack flank, and $\kappa = (3-\nu)/(1+\nu)$ for plane stress and $\kappa = 3-4\nu$ for plane strain. Equation (3) was

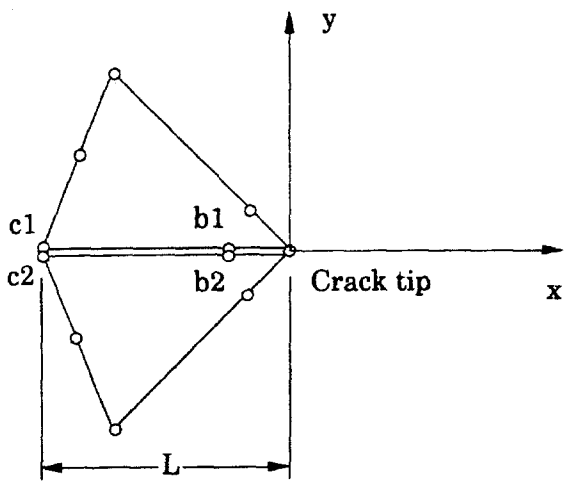

Fig. 7—Quarter-point elements at the crack tip

originally used in the finite element program's postprocessor once the displacement field was obtained. Because the moiré provides full-field displacements, the displacements required in this formula can be obtained here from the fringe pattern.

Equation (3) requires displacement data at the crack edge to compute the stress intensity factor. However, fringes close to the edge of the crack surface of Figs. 5 and 6 are very noisy. The smoothing finite element method was therefore used to smooth the moiré-measured displacement field beyond the immediate neighborhood of the crack. This smoothing FEM concept was then used to obtain reliable displacement data at the edge of the crack. Because the crack in the three-point bending beam is subjected to Mode I fracture, only displacements perpendicular to the crack surface were used (i.e., v displacements of Fig. 7). Details for experimentally evaluating the stress intensity factor by this approach are provided in Refs. 25, 30 and 31, and only the necessary salient aspects are covered here.

Consider a region R that encloses a crack (Fig. 8). Measured displacement data $\{v_k\}$ at any arbitrary locations $\{x_k y_k\}$ within R are represented throughout R by a smooth function $\{v\}$, which is obtained by minimizing the following functional matrix:

$$\{\phi\} = \left\{\frac{1}{2}\sum_{k=1}^{T}\alpha_K\left[v(x_K, y_K) - v_K\right]^2 + \frac{\varepsilon}{2}\int_R\left[v_{xx}^2 + 2v_{xy}^2 + v_{yy}^2\right]dR\right\}, \quad (4)$$

where T is total number of locations within R at which one inputs measured component of displacement, and ε is a smoothing parameter. Because it is almost impossible to solve eq (4) analytically, it is solved here by using the finite element method. Region R is discretized into eight-node plane isoparametric elements with the isoparametric coordinates denoted by ζ and η. The global coordinates $\{x\ y\}$ and the displacements $\{v\}$ within any individual element are defined as

$$x = \sum N_i x_i$$
$$y = \sum N_i y_i \tag{5}$$

and

$$v = \sum N_i v_i. \tag{6}$$

The shape functions are given by

$$N_i = \frac{1}{4}(1+\zeta\zeta_i)(1+\eta\eta_i)(\zeta\zeta_i+\eta\eta_i-1) \quad i=1,2,3,4$$
$$N_i = \frac{1}{2}(1+\zeta\zeta_i)(1-\eta^2) \qquad i=5,6 \tag{7}$$
$$N_i = \frac{1}{2}(1-\xi^2)(1+\eta\eta_i) \qquad i=7,8,$$

where ξ_i and η_i are the local isoparametric coordinates of the ith node. On substituting eqs (6) and (7) into eq (4) and minimizing the results with respect to $\{D\}$, which is the nodal displacement vector of the structure R in terms of global coordinates, one obtains

$$\sum_{j=1}^{M}[k_j]\{d_j\} = \sum_{j=1}^{M}\{p_j\}, \tag{8}$$

where

$$[k_j] = \sum_{i=1}^{T_j}\alpha_i[N_j(\xi_i,\eta_i)]^T[N_j(\xi_i,\eta_i)] + \varepsilon\int_{R_j}\left\{[N_j]_{xx}^T[N_j]_{xx} + 2[N_j]_{xy}^T[N_j]_{xy} + [N_j]_{yy}^T[N_j]_{yy}\right\}dR$$
$$\{p_j\} = \sum_{i=1}^{T_j}\alpha_i[N_j(\xi_i,\eta_i)]^T v_i. \tag{9}$$

M is the total number of elements used in the region R, and T_j is the total number of locations within the jth element where the measured displacements are input. On assembling the equations for all the elements, one obtains

$$[K]\{D\} = \{P\}, \tag{10}$$

where $[K]$ is a pseudo-stiffness matrix and $\{P\}$ is a pseudo-load vector that involves the moiré measured displacements. After solving this equation for $\{D\}$, the displacements can be computed throughout region R.

To smooth the moiré-measured displacements and evaluate reliable values of v on the crack flank for use in eq (3), the moiré fringes were digitized and the respective fringe orders were assigned. Displacements throughout the entire region R behind the crack tip of Fig. 8 were then obtained by converting fringe order to displacements [eq (1)]. Unreliable moiré data close to the edge of the crack were excluded. Region R (containing the moiré-measured displacements) of Fig. 8 was discretized into eight elements. The four elements immediately around the crack tip are quarter-point elements, and the others are eight-node serendipity quadrilateral elements.

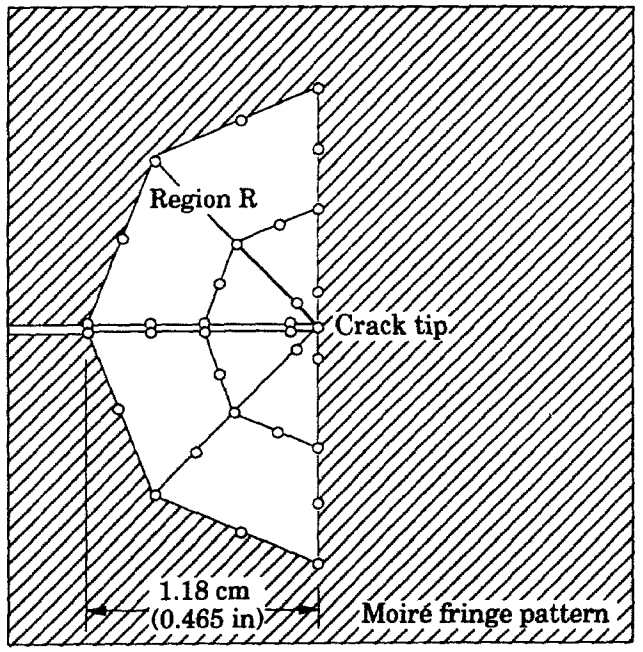

Fig. 8—Smoothing FEM mesh behind the crack tip

After smoothing the measured moiré data in region R, the stress intensity factor was obtained from eq (3). It is important to interpret the results correctly. Because eq (3) assumes LEFM, the computed K_I is reliable only if the fracture process zone is sufficiently small. For large FPZs, the stress intensity factor computed from eq (3) no longer corresponds to that for the original geometry of the specimen. However, eq (3) involves only the displacement field behind the crack tip, and the value obtained from the equation can be interpreted as the stress intensity factor of the same specimen but with different (longer) crack length. Consequently, the results can be used as a reference to assess the effect of the FPZ on K_I.

Results and Discussion

Moiré interferometry tests revealed fringe patterns surrounding the cracks in concrete and mortar beams. The fringes are isodisplacement contours. The discontinuity of a fringe pattern implies localized large deformation in the region. Fracture process zone, which is localized large deformation, can be observed directly from the fringe pattern in front of the crack tip. As mentioned in the previous sections, the fringes were recorded on sheet films and videotape. The recorded fringes provided information that was used to determine the relationship between FPZ length and the loading that caused the localized deformation. Our test results show that there is a large FPZ ahead of the crack tip before the load

TABLE 4—RESULTS FOR STRESS INTENSITY FACTOR K_I FOR MORTAR. M IS THE NUMBER OF INPUT MOIRÉ MEASURED DISPLACEMENTS

Loading N (lb)	M	K_I [eq (2)] kPa$\sqrt{m}$ (psi$\sqrt{in}$)	K_I [eq (3) and Moiré] kPa$\sqrt{m}$ (psi$\sqrt{in}$)	Discrepancy
1895	174	727.79	728.57	0.1 percent
(426)		(662.23)	(662.94)	
2135	203	820.04	1082.16	32.0 percent
(480)		(746.17)	(984.70)	
2277	222	874.72	1198.80	37.1 percent
(512)		(795.92)	(1090.81)	
2393	211	919.14	1960.02	113.2 percent
(538)		(836.34)	(1783.46)	

reaches maximum value. This large FPZ induces nonlinear stress-strain relation. The numerical results from smoothing FEM analysis verify the nonlinearity.

Table 4 contains the values of the stress intensity factor K_I based on the LEFM expression of eq (2), eq (3) and moiré-measured displacements. M is the number of measured moiré data used in the smoothing FEM analysis. At P = 1.90 kN (426 lb), the stress intensity factor computed from moiré is the same as that predicted by the LEFM formulation of eq (2). As the load increases, the size of the FPZ becomes larger. The difference between the values for K_I based on the two approaches also increases with increased FPZ. This result indicates that the size of the FPZ has a significant effect on the magnitude of the stress intensity factor.

With reference to eq (4) for the smoothing finite element approach, α_k was taken equal to 1 throughout this application to fracture of the three-point bending specimens. Also, the value of the smoothing parameter ε was determined in each case according to the approach suggested in Ref. 31. Representative values of ε used here range from 1.0e-5 to 1.0e-4. It is relevant to note that although eq (3) assumes linear elastic response, eqs (4) through (10) do not involve any assumptions regarding the constitutive behavior.

Conclusions

Moiré interferometry results reveal that a large fracture process zone can occur ahead of a crack tip in concrete/mortar. The size of this FPZ can significantly affect the magnitude of the stress intensity factor. The value of K_I based on the classical equation for a beam under three-point bending agrees well with that from moiré at the low loads where the damage zone ahead of the crack is small. However, the former becomes less reliable as the size of the damage zone increases. This is the first known application of hybridizing moiré-measured displacements in the neighborhood of a crack with finite elements to analyze the fracture process zone in an aggregate reinforced composite.

Acknowledgment

This research was funded by the National Science Foundation (BCS-8818230 and BCS-8819068), whose support is greatly appreciated.

References

1. *Hillerborg, A., Modeer, M. and Peterson, P.E., "Analysis of Crack Formation and Crack Growth in Concrete by Means of Fracture Mechanics and Finite Elements," Cement and Concrete Res.,* **6**, *773–782 (1976).*

2. *Bazant, Z.P. and Oh, B.H., "Crack Band Theory for Fracture of Concrete," Materiaux et Constructions,* **16** *(93), 155–177 (1983).*

3. *Gopalaratnam, V.S. and Ye, B.S., "Numerical Characterization of the Nonlinear Fracture Process in Concrete," Eng. Fract. Mech.,* **40** *(6) 991–1006 (1991).*

4. *Schorn, H. and Rode, U., "Numerical Simulation of Crack Propagation from Microcracking to Fracture," Cement & Concrete Composites,* **13**, *87–94 (1991).*

5. *Jefferson, A.D. and Wright, H.D., "Stepped Softening Functions for Concrete Fractures in Finite Element Analysis," Computer & Structures,* **41** *(2), 331–344 (1991).*

6. *Rots, J.G., "Smeared and Discrete Representations of Localized Fractures," Int. J. Fract.,* **51**, *45–59 (1991).*

7. *Brincker, R. And Dahl, H., "Fictitious Crack Model of Concrete Fracture," Magazine of Concrete Research,* **41** *(147), 79–86 (1989).*

8. *Gambarova, P.G. and Valente, G., "Smeared Crack Analysis for Fracture and Aggregate Interlock in Concrete," Eng. Fract. Mech.,* **35** *(4-5), 651–663 (1990).*

9. *Gerstle, W.H. and Xie, M., "FEM Modeling of Fictitious Crack Propagation in Concrete," ASCE J. Eng. Mech.,* **118** *(2), (1992).*

10. *Du, J., Kobayashi, A.S. and Hawkins, N.M., "Direct FEM Analysis of Concrete Fracture Specimens," ASCE J. Eng. Mech.,* **116** *(3), 605–619 (1990).*

11. *Du, J.J., Kobayashi, A.S. and Hawkins, N.M., "An Experimental-numerical Analysis of Fracture Process Zone in Concrete Fracture Specimens," Eng. Fract. Mech.,* **35** *(1-3), 15–27 (1990).*

12. *Guo, Z.K., Kobayashi, A.S. and Hawkins, N.M., "Further Studies on Fracture Process Zone for Mode I Concrete Fracture," Private Communication (1993).*

13. *Yu, C.T., Kobayashi, A.S. and Hawkins, N.M., "Energy Dissipation Mechanisms Associated with Rapid Fracture of Concrete,"* EXPERIMENTAL MECHANICS, **33** *(3), 205–211 (1993).*

14. *Chong, K.P., Li, V.C. and Einstein, H.H., "Size Effects, Process Zone and Tension Softening Behavior in Fracture of Geomaterials," Eng. Fract. Mech.,* **34** *(3), 669–678 (1989).*

15. *Karihaloo, B.L. and Nallathambi, P., "Effective Crack Model for the Determination of Fracture Toughness (K^e_{Ic}) of Concrete," Eng. Fract. Mech.,* **35** *(4-5), 637–645 (1990).*

16. *Whittmann, F.H. and Hu, X., "Fracture Process Zone in Cementitious Materials," Int. J. Fract.,* **51**, *3–18 (1991).*

17. *Jenq, Y.S. and Shah S.P., "A Fracture Toughness Criterion for Concrete," Eng. Fract. Mech.,* **21** *(5), 1055–1069 (1985).*

18. *Bistricic, L., Demoli, N. and Vukicevic, D., "Structural Behavior Investigations of Specially Light Concrete by Holographic Interferometry," SPIE Proc. Holography,* **1183**, *389–400 (1989).*

19. *Aassved Hansen, E., "A Holographic Real Time Study of Crack Propagation in Concrete," Cement and Concrete Res.,* **19**, *611–620 (1989).*

20. *Horii, H. and Ichinomiya T., "Observation of Fracture Process Zone by Laser Speckle Technique and Governing Mechanism in Fracture of Concrete," Int. J. Fract.,* **51** *19–29 (1991).*

21. Jia, Z. and Shah, S.P., "Two-dimensional Electronic Speckle Pattern Interferometry (2D-ESPI) and Concrete Fracture Processes," The International Conference on Nondestructive Testing of Concrete in the Infrastructure, Dearborn MI (1993).

22. Jankowski, L.J. and Stys, D.J., "Formation of the Fracture Process Zone in Concrete," Eng. Fract. Mech., **36** (2), 245–253 (1990).

23. Shao, Y., Li, Z. and Shah, S.P., "Micromechanical Study of Cement Composites by Moiré Interferometry," The International Conference on Nondestructive Testing of Concrete in the Infrastructure, Dearborn, MI (1993).

24. Post, D., "Moiré Interferometry," Handbook on Experimental Mechanics, ed. A.S. Kobayashi, VCH Publishers, New York (1993).

25. Feng, Z. and Rowlands, R.E., "Continuous Full-field Representation and Differentiation of Three-dimensional Experimental Vector Data," Computers & Structures, **26** (6), 979–990 (1987).

26. He, S., "Hybrid Experimental/numerical Analysis and Finite Element Modeling of Fracture of Aggregate Composite," Ph. D. thesis, Department of Engineering Mechanics, University of Wisconsin-Madison (1993).

27. Broek, D., Elementary Engineering Fracture Mechanics, Martinus Nijhoff, The Hague (1982).

28. Barsoum, R.S., "On the Use of Isoparametric Finite Elements in Linear Fracture Mechanics," Int. J. Numerical Methods Eng., **10**, 25–37 (1976).

29. Saouma, V.E. and Schwemmer, D., "Numerical Evaluation of the Quarter-point Crack Tip Element," Int. J. Numerical Methods Eng., **20**, 1629–1641 (1984).

30. Feng, Z., Sanford, R.J. and Rowlands, R.E., "Determining Stress Intensity Factors from Smoothing Finite-element Representation of Photomechanical Data," Eng. Fract. Mech., **40** (3), 593–601 (1991).

31. Segalman, D.J., Woyak, D.B. and Rowlands, R.E., "Smooth Spline-like finite-element Differentiation of Full-field Experimental Data over Arbitrary Geometry," EXPERIMENTAL MECHANICS, **19** (12), 429–437 (1979).